Universiteit
Leiden
The Netherlands

Soil organic amendments for climate-smart agriculture

Kok, D.D.

Citation
Kok, D. D. (2024, September 26). *Soil organic amendments for climate-smart agriculture*. Retrieved from https://hdl.handle.net/1887/4093453

Version:	Publisher's Version
License:	Licence agreement concerning inclusion of doctoral thesis in the Institutional Repository of the University of Leiden
Downloaded from:	https://hdl.handle.net/1887/4093453

Note: To cite this publication please use the final published version (if applicable).

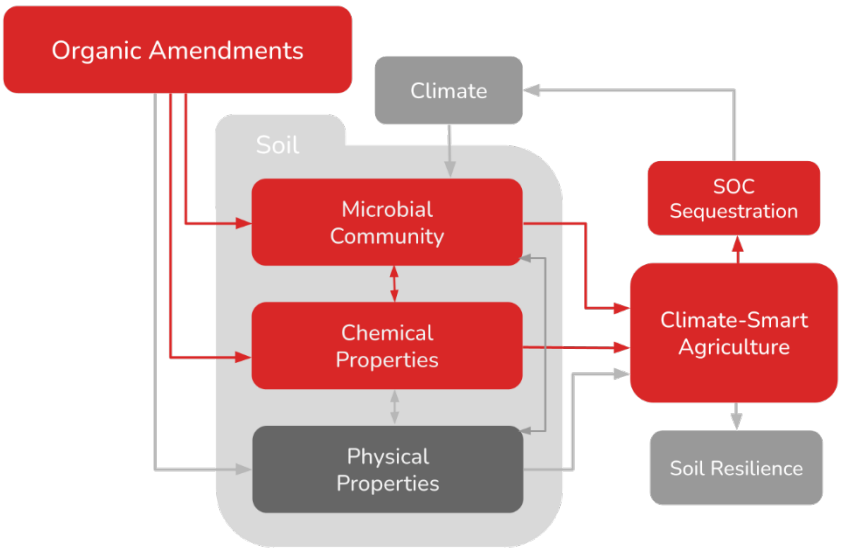
Organic Amendments
Climate
Soil
Microbial Community
Chemical Properties
Physical Properties
SOC Sequestration
Climate-Smart Agriculture
Soil Resilience

CHAPTER 3

MiPrime: A Soil Model for the Microbially Mediated Impacts of Organic Amendments on Measurable Carbon Fractions and Associated Priming Effects

Dirk-Jan Kok
Laura Scherer
Wim de Vries
Peter van Bodegom

Under review by *Soil Biology and Biochemistry (2024)*.

ABSTRACT

Priming effects can influence the efficiency with which organic amendments sequester carbon in the soil. Yet few contemporary soil models include priming effects, while those that do often involve operationally defined soil pools that inhibit the verification of model processes with experimental data. To address these shortcomings, we developed the MiPrime model, which offers a framework for the mechanistic modelling of organic amendment impacts on microbially mediated transformation of carbon fractions that are quantifiable through parsimonious soil extraction methods. MiPrime allows for assessment of organic amendment impacts on soil carbon dynamics, including priming effects, by simulating changes in mineralized, microbial biomass, dissolvable, hot water extractable and insoluble carbon fractions in soil exogenous (i.e. organic amendment-derived) and endogenous (i.e. soil) pools. After calibration of model parameters using Markov Chain Monte Carlo methods to incubation data of three types of isotopically labelled roadside grasses (a fresh grass product, a compost thereof, and a Bokashi-fermented product thereof), MiPrime was able to simulate changes in carbon fractions of the soil with a good degree of accuracy for five compositionally complex organic amendments, namely the three types of roadside grasses, as well as non-isotopically labelled wood chips and water weeds and reeds. Validation of the model results with experimental data demonstrates that changes in total carbon were very well predicted but that there is room for improvement in predicting mineralization rates and changes in dissolvable, hot water extractable and insoluble carbon fractions in the soil endogenous pool. MiPrime thus offers an initial step towards the mechanistic modelling of organic amendment impacts on measurable soil carbon fractions and can operate as a new tool for designing effective carbon sequestration strategies and understanding organic amendment impacts.

The presented data has been made publicly accessible in the DANS-Easy data repository under 10.17026/dans-zp3-haqt

Keywords: *organic amendments, soil carbon modelling, decomposition, soil microbial community, priming effect*

3.1 INTRODUCTION

Soil organic matter (SOM) constitutes the largest pool of terrestrial carbon on Earth (Smith 2012; Stockmann et al. 2013). It regulates several soil functions related to agricultural production and climate change mitigation and is, therefore, of considerable interest in soil management (Lal 2016; Magdoff and Weil 2004). The accumulation of SOM is a long-term process, but it can be facilitated through the application of organic amendments (Goyal et al., 1999; Paustian et al., 1992). Especially in agricultural settings, organic amendments can substitute or supplement soil-deprived influxes of organic matter due to crop residue removal and thereby offset carbon lost through decomposition (Blanco-Canqui and Lal 2009; Diacono and Montemurro 2011). Furthermore, by contributing to accumulating and preserving SOM, organic amendments can recuperate soils degraded under conventional agro-industrial practices and sustainably improve agricultural productivity (Karlen and Rice 2015; Lal 2016).

However, our limited ability to accurately predict the impacts of organic amendments inhibits the design and implementation of effective and efficient organic amendment application strategies. Organic amendment impacts are difficult to predict, as they are influenced by both the quantity (i.e. application rate) and quality (e.g. chemical and physical properties) of the amendments applied and their complex interaction with local soil fauna and microorganisms. The many relevant soil biotic and abiotic factors affecting these microbial responses further complicate this prediction (Allison et al. 2013; Benbi and Khosa 2014; Kirkby et al. 2014; Li et al. 2014; Schimel and Schaeffer 2012; Sierra et al. 2015).

Recent technological and methodological advances in soil and organic matter analysis (Kögel-Knabner 2017; Kögel-Knabner and Rumpel 2018) have shed new light onto the intricate relationships between soil carbon dynamics, organic amendment composition, microbial properties and processes, and environmental factors (e.g. soil texture, acidity and humidity; (Allison, Wallenstein, and Bradford 2010; Manzoni et al. 2018; Moorhead and Sinsabaugh 2006; Schimel and Weintraub 2003). These insights have considerably improved our understanding and ability to predict the impact of different organic amendments in the field situation and have led to the development of a new generation of soil carbon models that include explicit representations of microbial processes and mechanisms regulating decomposition through, for instance, second-order decay dynamics, such as in DEMENT (Allison 2014), DAMM (Davidson, Savage, and Finzi 2014), BAMS1 (Dwivedi et al. 2017; Riley et al. 2014), CORPSE (Sulman et al. 2014), MIMICS (Wieder et al. 2014), MEND (G. Wang et al. 2015), PRIM (Guenet et al. 2016), Millennial

(Abramoff et al. 2018), ORCHIMIC (Huang et al. 2018), and C-Stability (Sainte-Marie et al. 2021).

The new generation of decomposition models is a milestone in the development of our understanding of soil carbon dynamics and our ability to predict changes therein. However, important mechanisms driving organic amendment impacts on soil carbon dynamics are often still elusive and, therefore, also remain neglected in most of these new models. For instance, changes in the decomposition rate of endogenous organic matter following the application of organic amendments, i.e. priming effects, are often neglected or not explicit. Yet, priming effects can affect the efficiency with which soil carbon can be accumulated or sequestered (Wang et al. 2022). Priming effects can, for example, be positive, accelerating the decomposition of endogenous organic matter, or negative, reducing its decomposition rates (Bastida et al. 2017; Guenet et al. 2010; Hamer and Marschner 2005b; D. D. Kok et al. 2022; Yu et al. 2020). For the purpose of carbon sequestration and building SOM stocks, negative priming effects are desirable. The direction and magnitude of priming effects vary for different organic amendments, yet relationships of this variation with the quantity and quality of the organic amendments and other soil properties remain difficult to establish (H. Wang et al. 2015). Consequently, priming effects are poorly represented in soil models. Where priming effects are included, it is often only implicitly, allowing for solely positive priming effects through the natural increase in the biomass pool as a result of a great abundance of feeding substrate. These model limitations constrain the potential use of these models for designing and assessing optimal organic amendment application strategies.

In addition to predicting organic amendment impacts in the field situation (practical application value), models can also offer important insight into the potential biogeochemical mechanisms that drive changes in soil properties (scientific value). Limiting a model's potential value in this regard, however, is the frequent adherence to operationally defined characterizations of organic matter quality, i.e. as fractions of 'slow', 'fast' and 'passive' carbon. While simplifying model testing, improving tractability and thereby benefiting model application, operationally defined organic matter pools diminish a model's potential contribution to developing our understanding of carbon dynamics (Abramoff et al. 2018; Elliott, Paustian, and Frey 1996). Despite calls to 'model the measurable' and 'measure the modellable' already in the previous century (Christensen 1996; Elliott et al. 1996), operationally defining organic matter fractions remains popular which contributes to a growing "disconnect between those scientific communities working to understand the chemistry of SOM on a mechanistic basis and those that are more concerned with applied questions of land management and have a need for operational metrics" (Kleber and Johnson 2010).

Defining pool sizes, turnover rates, and transfer coefficients based on metrics that can be directly measured or acquired from empirical data allows models to retain their field

application potential while simultaneously providing much more insight into the underlying mechanisms that drive changes in the soil (Todd-Brown et al. 2012). Empirical findings, for instance, have demonstrated how the directly-measurable chemical heterogeneity of organic matter inputs are directly related to the degree and direction of priming effects (Leiyi Chen et al. 2019; D. D. Kok et al. 2022:2; Liu et al. 2020). Distinguishing differences in organic matter quality based on such measurable biogeochemical fractions (Wang et al., 2015) and/or potentially their depolymerization continuums (Sainte-Marie et al. 2021) offers more meaningful insight into the interactions between microorganisms and organic matter chemistry than defining these relationships based on somewhat ambiguous pools of 'labile' and 'recalcitrant' carbon. Furthermore, as the changes in different organic matter quality pools can be monitored throughout decomposition, such characterizations also allow for more robust validation of model processes. Yet, all of the aforementioned models that allow for the explicit assessment of priming effects, i.e. PRIM and ORCHIMIC, do so only through operationally defined characterizations of organic matter fractions. These models follow a traditional CENTURY model framework, distinguishing between differences in organic matter quality based on 'metabolic' and 'structural' fractions for organic amendments and 'active', 'slow' and 'passive' fractions for soil endogenous organic matter (Guenet et al. 2016:20; Huang et al. 2018; Parton et al. 1987).

To address this shortcoming, we present the '**MI**crobially mediated **PRI**ming effects model with **ME**asurable organic carbon pools' (MiPrime). MiPrime allows for the simulation and prediction of the immediate, microbially mediated impacts of different organic amendments on soil carbon dynamics, including their priming effects, wherein changes in different measurable organic matter fractions are largely verifiable following parsimonious organic matter fractionation procedures. Thereby, MiPrime contributes to bridging the gap between applied and theoretic soil sciences, operating as a new potential tool for both designing carbon sequestration strategies and understanding the mechanisms driving organic amendment impacts.

3.2 MATERIALS AND METHODS

3.2.1 Model design

MiPrime employs a multi-compartmental framework that distinguishes between endogenous organic matter (EN) pools already present in the soil and exogenous organic matter (EX) pools recently applied in the form of litter or an organic amendment. The organic matter quality of these pools is subsequently described based on their readily dissolvable (D), hot-water extractable (H), and insoluble/acid non-hydrolysable (I) fractions with their carbon concentrations (Figure 3.1). These fractions in the EN and EX pools are experimentally measurable, where pool separation can be realized through well-established isotope labelling techniques (Amelung et al. 2008), and organic matter quality fractionation can be achieved largely by applying a series of chemical extraction protocols to isolate D, H and I (D. D. Kok et al. 2022).

In the MiPrime model, the decomposition of D, H and I fractions (see Figure 2) in both endogenous and exogenous organic matter is controlled by biological processes following Michaelis-Menten-type functions. Over time, as soil microorganisms interact with each fraction, a portion of its mass is incorporated into microbial biomass, mineralized in the form of microbial-growth respiration, and transformed into extracellular microbial products (e.g. exoenzymes, polymers, proteins and/or mucilages). Priming effects are modelled to occur as a result of an increase in microbial activity and the enzymatic preference for either endogenous or exogenous carbon depending on the difference in concentration of that fraction between the exogenous and endogenous pools (D. D. Kok et al. 2022). Model parameter values and uncertainties were determined through Bayesian inference and Markov Chain Monte Carlo methods applied to data derived from a 160-day incubation experiment applying natural, isotopically labelled organic amendments (D. D. Kok et al. 2022). We present a comparison of simulated versus observed data from a dataset for different amendments of the same incubation experiment and perform a parameter sensitivity analysis using Fourier Amplitude Sensitivity Testing (FAST).

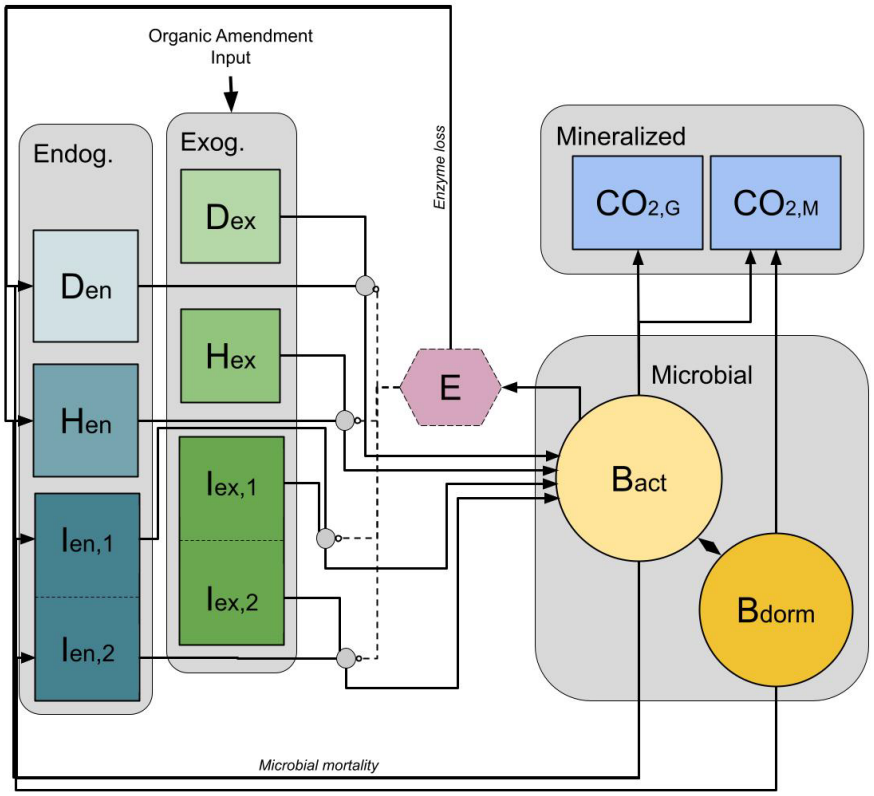

Figure 3.1. MiPrime conceptual design. Solid lines illustrate carbon fluxes, and dotted lines illustrate moderation effects. Components with solid boundaries indicate parametrization based on measured data. D_{en}, H_{en}, and $I_{en,(1,2)}$ and D_{ex}, H_{ex}, and $I_{ex,(1,2)}$ represent dissolvable, hot water extractable, and insoluble carbon fractions ($I_{en/ex,1}$ being the rapid subcomponent and $I_{en/ex,2}$ the slower one) of the endogenous (EN) and exogenous (EX) organic matter pools, respectively; E represents the extracellular microbial products mediating the decomposition of D, H and I fractions within each pool; B_{act} is the total active microbial biomass; B_{dorm} is the dormant microbial biomass; and *Mineralized* is the sum of accumulated microbial growth ($CO_{2,G}$) and maintenance ($CO_{2,M}$) respiration.

MiPrime recalculates the mass of each organic matter fraction, per pool, at a daily time step over the course of decomposition. A change in the mass of each fraction is determined based on its state in the previous time step and the difference between its influxes and effluxes. These influxes and effluxes are defined differently per EX and EN pool, as, over time, EX organic matter is allowed to gradually transform into EN organic matter, but not the other way around (Figure 3.1). This transformation from EX to EN occurs through the assimilation of EX carbon in microbial biomass and subsequent transformation into abiotic EN organic matter as microbial necromass due to microbial mortality. A system of non-linear differential equations was constructed to describe the changes in the organic matter

fractions for EX (eq. 3.1) and EN pools (eq. 3.2), microbial biomass that is active (eq. 3.3) and dormant (eq. 3.4), microbial extracellular products (eq. 3.5), microbial respiration (eq. 3.6), and primed carbon (eq. 3.7).

$$\frac{dF^{ex}}{dt} = -F_{dec}^{ex} + F_{in}^{ex} \qquad F^{ex} \in \{D^{ex}, H^{ex}, I^{ex}\} \tag{3.1}$$

$$\frac{dF^{en}}{dt} = -F_{dec}^{en} + \left(B_{mort}^{act} + B_{mort}^{dorm}\right) \cdot p_{B,F} + 0.33 * E_{loss}^{F} \qquad F^{en} \in \{D^{en}, H^{en}, I^{en}\} \tag{3.2}$$

$$\frac{dB^{act}}{dt} = \sum_{F=D,H,I} (F_{dec}^{ex} + F_{dec}^{en}) - B_{to\_dorm}^{act} + B_{to\_act}^{dorm} - B_{resp}^{act} - \sum_{F=D,H,I} E_{synth}^{F} \tag{3.3}$$

$$\frac{dB^{dorm}}{dt} = B_{to\_dorm}^{act} - B_{to\_act}^{dorm} - B_{resp}^{dorm} \tag{3.4}$$

$$\frac{dE^{F}}{dt} = E_{synth}^{F} - E_{loss}^{F} \tag{3.5}$$

$$\frac{dCO_2}{dt} = B_{resp}^{act} + B_{resp}^{dorm} \tag{3.6}$$

$$\frac{dPE}{dt} = \frac{dCO_2{}^{en,amended}}{dt} - \frac{dCO_2{}^{en,conrol}}{dt} \tag{3.7}$$

The functions describing these changes are summarized in Table 3.1, with 31 associated parameters, of which 28 are fitted and 3 are fixed, whose description and prior information are summarized in Table 3.2. Principally, the decomposition of each fraction is calculated by applying a reverse Michaelis-Menten function (eq. 3.8, 3.9), which is furthermore modified by the affinity of extracellular products (eq. 3.10) for either the EX or EN pool based on the difference in the hot-water extractable carbon concentration of each pool (D. D. Kok et al. 2022). Proportions of the microbial biomass that is active or dormant depends on the total concentration of organic carbon (eq. 3.12). Respiration rate of active microorganisms (eq. 3.13) is driven by the rate of decomposition (eq. 3.14) and microbial maintenance requirements (eq. 3.15) whereas respiration rates for dormant microorganisms are only driven by their maintenance (eq. 3.16). Microbial mortality is defined as constant fraction of the total maintenance requirement for active (eq. 3.17) and dormant microbial populations (eq. 3.18). By attributing a constant use-efficiency to each carbon fraction, the

model allows for a dynamic assessment of amendment use-efficiency by microbes based on differences in amendment composition and how this composition changes over the course of decomposition. The MiPrime model is largely inspired by MEND (Wang et al., 2015) and YASSO (Liski et al. 2005), from which we have adopted and modified many functions to fit the representation of organic matter and our interpretation of microbial-organic matter interactions. To avoid overparameterization and equifinality issues, we chose to fix three parameters. These were selected because they are of relatively limited interest in this study (β: dormant microbial modifier; r_0: initial proportion of active versus dormant microorganisms) and/or are easily deduced from the data ($S_{I2,ex}$: size of the I_2 fraction in the amendments; deduced from Appendix Figure B2). The 0.05 modifier for dormant microbes was picked to be within the range for dormant versus active ratio of maintenance respiration reported by (Wang et al. 2014); 0.025-0.351).

Table 3.1. Functions in the MiPrime model. Parameters are described in Table 3.2.

Flux description	Equation	
Decomposition of exogenous pool carbon fractions. $F \in \{D, H, I\}$	$F_{dec}^{ex} = q_F \cdot F^{ex} \cdot \frac{\left(E^F \cdot (1 - A^F)\right)}{\left(E^F \cdot (1 - A^F)\right) + K_F}$	(3.8
Decomposition of endogenous pool carbon fractions. $F \in \{D, H, I\}$	$F_{dec}^{en} = q_F \cdot F^{en} \cdot \frac{\left(E^F \cdot (1 + A^F)\right)}{\left(E^F \cdot (1 + A^F)\right) + K_F}$	(3.9
Microbial affinity factor for fraction $F \in \{D, H, I\}$ and in each pool $P \in \{ex, en\}$.	$A^F = \tau \cdot \left[\frac{H^{ex}}{T^{ex}} / \left(\frac{H^{ex}}{T^{ex}} + \frac{H^{en}}{T^{en}}\right) - 0.5\right]^{\gamma}$ And $T^P = \sum F^P$	(3.10
Dormancy ($B_{to\_dorm}^{act}$) and reactivation ($B_{to\_act}^{dorm}$) between active (B^{act}) and dormant (B^{dorm}) microbial biomass.	$B_{to\_dorm}^{act} = \left(1 - \frac{T^{ex} + T^{en}}{T^{ex} + T^{en} + K_{dorm}}\right) \cdot \alpha_B \cdot B^{act}$ $B_{to\_act}^{dorm} = \left(\frac{T^{ex} + T^{en}}{T^{ex} + T^{en} + K_{dorm}}\right) \cdot \alpha_B \cdot B^{dorm}$	(3.11 (3.12
Respiration by active biomass (B_{resp}^{act}) during substrate consumption ($B_{resp\_G}^{act}$) and base maintenance ($B_{resp\_m}^{act}$). $F \in \{D, H, I\}$	$B_{resp}^{act} = B_{Resp\_G}^{act} + B_{Resp\_m}^{act}$ $B_{resp\_G}^{act} = \sum_F (1 - \eta_F) \cdot (1 - \eta_E) \cdot (F_{dec}^{ex} + F_{dec}^{en})$ $B_{resp\_m}^{act} = p_R \cdot m_r \cdot B^{act}$	(3.13 (3.14 (3.15
Respiration by dormant biomass (B_{resp}^{dorm}) for base maintenance.	$B_{resp}^{dorm} = p_R \cdot m_r \cdot B^{dorm} \cdot \beta$	(3.16
Mortality of active (B_{mort0}^{act}) and dormant biomass (B_{mort}^{dorm})	$B_{mort}^{act} = (1 - p_R - p_E) \cdot m_r \cdot B^{act}$ $B_{mort}^{dorm} = (1 - p_R - p_E) \cdot m_r \cdot B^{dorm} \cdot \beta$	(3.17 (3.18
Extracellular product synthesis during substrate consumption ($E_{Syn\_G}^F$) and basal extracellular product synthesis as maintenance ($E_{Syn\_m}^F$)	$E_{Synth}^F = E_{Syn\_G}^F + E_{Syn\_m}^F$ $E_{Syn\_G}^F = (1 - \eta_F) \cdot \eta_E \cdot (F_{dec}^{ex} + F_{dec}^{en})$ $E_{Syn\_m}^F = 0.33 \cdot p_E \cdot m_r \cdot B^{act}$	(3.19 (3.20 (3.21
Extracellular product loss. $F \in \{D, H, I\}$	$E_{loss}^F = r_E \cdot E^F$	(3.22

Table 3.2. Parameters and prior information for the MiPrime model. U(a,b) denotes a uniform distribution between limits 'a' and 'b'.

Param.	Description	Prior	Unit
q_D	Maximum specific decomposition rate for *D*	U(0, 1)	μg C μg^{-1} soil d^{-1}
q_H	Maximum specific decomposition rate for *H*	U(0, 1)	μg C μg^{-1} soil d^{-1}
$q_{I,1}$	Maximum specific decomposition rate for I_1	U(0, 1)	μg C μg^{-1} soil d^{-1}
$q_{I,2}$	Maximum specific decomposition rate for I_2	U(0, 0.01)	μg C μg^{-1} soil d^{-1}
K_D	Half-saturation constant for *D* decomposition	U(0, 500)	μg C g^{-1} soil
K_H	Half-saturation constant for *H* decomposition	U(0, 500)	μg C g^{-1} soil
$K_{I,1}$	Half-saturation constant for I_1 decomposition	U(0, 500)	μg C g^{-1} soil
$K_{I,2}$	Half-saturation constant for I_2 decomposition	U(0, 5000)	μg C g^{-1} soil
η_D	Yield efficiency for decomposition of D	U(0, 1)	μg C μg^{-1} C
η_H	Yield efficiency for decomposition of H	U(0, 1)	μg C μg^{-1} C
$\eta_{I,1}$	Yield efficiency for decomposition of I_1	U(0, 1)	μg C μg^{-1} C
$\eta_{I,2}$	Yield efficiency for decomposition of I_2	U(0, 1)	μg C μg^{-1} C
η_E	Enzyme production efficiency from decomp.	U(0, 1)	μg C μg^{-1} C
m_R	Specific basal maintenance rate of B_{act}	U(0, 1)	μg C μg^{-1} C h^{-1}
p_E	Fraction of m_R for production of *E*	U(0, 1)	-
p_R	Fraction of m_R for respiration	U(0, 1)	-
p_M	Fraction of m_R for mortality	U(0, 1)	-
β	Dormant microbial modifier	0.05	-
r_E	Loss rate of *E*	U(0, 0.5)	μg C μg^{-1} C d^{-1}
K_{dorm}	Half-saturation constant for organic matter influencing reactivation and dormancy	U(0, 5000)	μg C g^{-1} soil
p_{BD}	Fraction of biomass that is D	U(0, 1)	μg C μg^{-1} C
p_{BH}	Fraction of biomass that is H	U(0, 1)	μg C μg^{-1} C
p_{BI1}	Fraction of biomass that is I_1	U(0, 1)	μg C μg^{-1} C
p_{BI2}	Fraction of biomass that is I_2	U(0, 1)	μg C μg^{-1} C
τ	Sensitivity of E to affinity for *ex* or *en* pool	U(0, 1)	-
γ	Trend modifier to the influence of concentration differences in H on affinity	U(0, 1)	-
Parameters for initialization			
r_0	Initial proportion of active vs. dormant microbes;	0.9	-
pE_D	Initial fraction of extracellular product in D_N	U(0, 1)	-
pE_H	Initial fraction of extracellular product in H_N	U(0, 1)	-
$S_{I2,ex}$	Total size of the I_2 fraction in the amendments.	1800	μg C μg^{-1} C
$p_{I2,en}$	Proportion of soil I that hardly decomposes on short timescales (I_2)	U(0.9, 1)	μg C μg^{-1} C

MiPrime models the decomposition of total organic carbon as the sum of changes in individual soil carbon solubility fractions (D, H and I). These fractions, however, are not chemically homogeneous and can contain components that are differently decomposable by microorganisms. Experimental findings show the I fraction consists of a rapidly decomposing component and a much slower one (Figure 3.4.1). To account for this

heterogeneity, MiPrime separates the I pool into two parts, I_1 and I_2 each with its own decomposition parameters. A conceptual illustration of the further componential breakdown of the carbon fractions in the MiPrime model is presented in Figure 3.2.

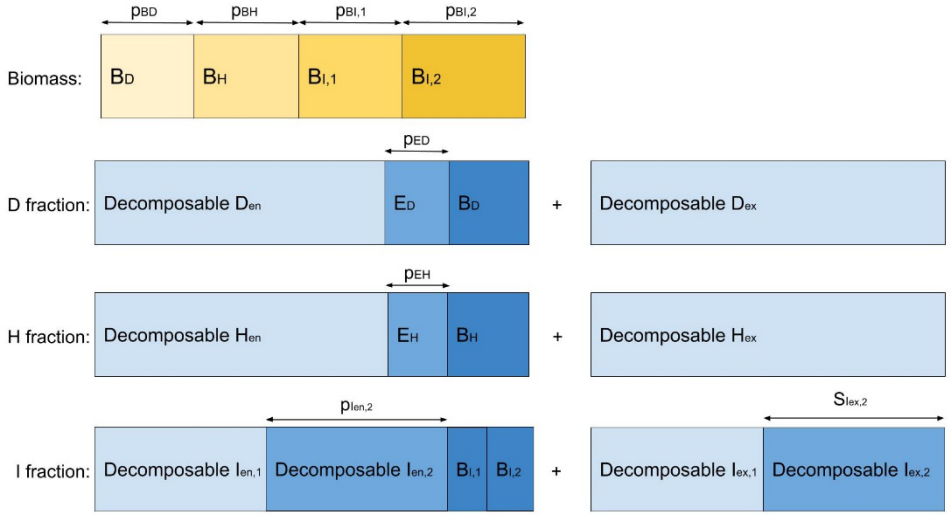

Figure 3.2. Conceptual illustration of the breakdown of different modelled carbon fractions and their components, as well as the parameters relevant to their initialization. The sizes of the boxes are arbitrary and do not reflect the actual sizes of these fractions and components.

Due to lacking laboratory procedures for measuring the sizes of these components, the MiPrime model initializes them by fitting parameters for i) the microbial biomass attributed to each D_{en}, H_{en} or I_{en} fraction (p_{BD}, p_{BH}, $p_{BI,1}$ and $p_{BI,2}$), ii) the initial extracellular product concentrations in D and H (pE_D, pE_H) and iii) for the size of the I_2 fraction in the soil pool ($pI_{en,2}$). The size of the I_2 fraction in the amendment pool was manually set based on observed asymptotes for the short-term decomposition of I around 1800 µg C g^{-1} soil for our three amendments (Figure 3.4.1). The following equations define MiPrime's estimation of decomposable fractions based on these considerations (measured data is emboldened):

$$D_{en} = \left[\boldsymbol{D_{en,meas}} - \boldsymbol{B} \cdot p_{BD}\right] \cdot [1 - pE_{ED}] \quad (3.23$$

$$H_{en} = \left[\boldsymbol{H_{en,meas}} - \boldsymbol{B} \cdot p_{BH}\right] \cdot [1 - pE_{EH}] \quad (3.24$$

$$I_{en} = I_{en,1} + I_{en,2} \quad (3.25$$

$$I_{en,1} = \left[\boldsymbol{I_{en,meas}} * (1 - p_{I2,en}) - \boldsymbol{B} \cdot p_{BI,2}\right] \quad (3.26$$

$$I_{en,2} = \left[\boldsymbol{I_{en,meas}} * p_{I2,en} - \boldsymbol{B} \cdot p_{BI,1}\right] \quad (3.27$$

$$D_{ex} = \boldsymbol{D_{ex,measured}} \quad (3.28$$

$$H_{ex} = \boldsymbol{H_{ex,measured}} \quad (3.29$$

$$I_{ex} = I_{ex,1} + I_{ex,2} \quad (3.30$$

$$I_{ex,1} = \left(\boldsymbol{I_{ex,measured}} - S_{I2,ex}\right) \quad (3.31$$

$$I_{ex,2} = S_{I2,ex} \quad (3.32$$

3.2.2 Experimental data for model calibration and validation

Model data for calibration and validation was derived from an experiment described in Kok et al. (2022). In summary, Podzol soil was acquired from an agricultural site in Haarlo, the Netherlands (52.10 N, 6.59 E) and incubated at 50 g per pot with 0.5 g (d.w.e.) of organic amendments with isotopically enriched carbon (^{13}C), namely i) roadside grasses, ii) compost from roadside grasses and iii) Bokashi-fermented roadside grasses, as well as with organic amendments of natural isotope abundance: iv) woodchips and v) waterway weeds and reeds. All amendments were cut or sieved to reduce their size to a maximum of 2 cm. Triplicate (n=3) incubation pots, for each organic amendment treatment and each sampling moment (t=3, 7, 16, 30, 60 and 150 days), were destructively sampled in their entirety to determine i) total microbial biomass carbon by chloroform-fumigation (Brookes et al. 1985; Vance et al. 1987), ii) carbon respiration activity by headspace sampling, and organic carbon fractions that are iii) dissolvable (D), hot-water extractable (H), and insoluble (I) by stepwise, wet-chemical extraction. Total carbon concentrations were calculated based on measurement of the initial carbon concentration minus cumulative carbon respiration rates. Priming rates were calculated as the difference in endogenous carbon respired between the amended soils and an unamended control soil. Data for the isotopically labelled organic amendments were used as model calibration data, whereas data for the non-labelled organic amendments were used for the validation of model predictions for total soil carbon, respired carbon, microbial biomass, dissolvable, hot-water extractable and insoluble carbon. Priming effects could not be validated as these cannot be calculated from organic amendments that are not isotopically enriched. Concentrations of exogenous and endogenous carbon in the incubation pots at the start of the experiment are summarized in Table 3.3.

Table 3.3. Endogenous and exogenous carbon concentrations, per carbon fraction, at the start of the experiment.

	Endog.	**Exogenous**				
	Soil	**Calibration Amendments**			**Validation Amendments**	
	Base	**Unproc. Grasses**	**Compost Grasses**	**Bokashi Grasses**	**Wood Chips**	**Waterway Residues**
	[µg g^{-1} soil]	[µg g^{-1} soil]	[µg g^{-1} soil]	[µg g^{-1} soil]	[µg g^{-1} soil]	[µg g^{-1} soil]
C_{TOT}	16,528±5	3,668±1	2,515±4	3,695±1	4,699±6	3,788±8
C_{IS}	1,5545±5	2,946±1	1,934±4	3,350±1	4,389±6	3,427±8
C_{HW}	929±93	298±16	331±19	168±3	265±4	239±6
C_{DO}	54±4	424±30	249±7	178±7	45±3	122±9

3.2.3 Bayesian calibration of model parameter values

Model parameters were calibrated through Bayesian methods using the calibration dataset. Each model parameter was assigned an approximated prior probability distribution $p(\theta)$ that was then combined with a multi-objective Gaussian likelihood function to provide a posterior distribution $p(\theta|y) \propto p(\theta)p(y|\theta) = p(\theta)\prod_i p(y_i|\theta)$; where observed data y constitutes our measured properties, namely the total, endogenous and exogenous derived carbon in biomass, and D, H, I, fractions, the mineralized pool and observed priming effects. Priming effects were attributed extra weight (factor 5) to ensure its prioritization in the parametrization. With 19 calibration variables of equal weight, the model attributes a ~4% interest ($\frac{1}{19}$) to getting the trend right for each. Increasing the weight of the priming variable in the likelihood function by a factor of five results in a 22% interest ($\frac{5}{18+1*5}$) in getting priming right and 78% for the combined other variables. For fractional parameters (e.g. microbial biomass composition p_{BD}, p_{BH}, etc.), values were used as parameters of a Dirichlet distribution whereby the mean values of these Dirichlet distributions (which always sum to 1) were taken as the actual parameter values implemented in the model. In the parametrization, the prior distribution of each model parameter was kept general and non-informative to attribute maximum power to the sampler and the data in determining the posterior. To derive useful information from our posterior distribution, we evaluated the posterior probability density function by Markov Chain Monte Carlo (MCMC) methods. By generating an ensemble of ten sampling chains that stochastically explore the parameter space through a random walk, we collected solutions of stable frequency to steer the walk in the direction of the posterior's better-fitting parameter values. To steer this random walk, we applied the DiffeRential Evolution Adaptive Metropolis with discrete sampling (DREAM) algorithm, a metropolis-type sampler specifically designed to explore complex, potentially multimodal, posterior

distributions for models of highly nonlinear water, energy, nutrient, and vegetation processes (Vrugt et al. 2008; Vrugt and Braak 2011). The DREAM sampler updated the state of each sampling chain with each draw, until convergence was achieved for each parameter across the ten chains. This convergence was tested through the Gelman-Rubin diagnostic, where convergence is considered achieved at diagnostic values lower than 1.2, as per package default (Houska et al. 2015). Once all parameters for all sampling chains had converged, 1,000 additional samples were drawn. We then determined the final parameter distributions based on samples with the highest likelihoods (top 10%) drawn after convergence. Finally, subsequent to parameter inference, we evaluated parameter sensitivity through a Fourier Amplitude Sensitivity Test (FAST). The Bayesian inference and sensitivity tests were implemented in Python using the Statistical Parameter Optimization Tool for Python (SPOTPY; Houska et al., 2015). The resulting distributions for each parameter are presented in Table 3.4. Associated graphs of the parameter trace and histograms of parameter values are presented in Supplementary Figure M1.

Table 3.4. Posterior mean, 95% Bayesian credibility intervals, and best parameter estimate for MiPrime model parameters. The 'Best' parameter value is the value that was assigned to a parameter which produced the highest likelihood value from all model runs.

Parameter (θ)	Units	2.5% Conf.	Mean	97.5% Conf.	Best
q_D	µgC µg^{-1}d^{-1}	0.161	0.384	0.834	0.319
q_H	µgC µg^{-1}d^{-1}	0.093	0.531	0.933	0.101
q_{I1}	µgC µg^{-1}d^{-1}	0.454	0.787	0.966	0.967
q_{I2}	µgC µg^{-1}d^{-1}	0.002	0.006	0.009	0.004
K_D	µgC g^{-1}	12.10	123.48	452.01	39.78
K_H	µgC g^{-1}	139.52	359.88	484.07	60.20
K_{I1}	µgC g^{-1}	289.22	413.04	495.19	335.8
K_{I2}	µgC g^{-1}	434.7	1325.7	3067.7	998.0
η_D	µgC µg^{-1}C	0.073	0.460	0.958	0.736
η_H	µgC µg^{-1}C	0.667	0.877	0.986	0.786
η_{I1}	µgC µg^{-1}C	0.007	0.085	0.253	0.004
η_{I2}	µgC µg^{-1}C	0.025	0.300	0.836	0.281
η_E	µgC µg^{-1}C	0.009	0.053	0.102	0.010
m_R	µgC µg^{-1}C d^{-1}	0.098	0.241	0.403	0.141
p_{E*}	-	2.977	7.209	9.750	9.337
p_{R*}	-	4.657	7.577	9.749	9.376
p_{M*}	-	2.236	7.298	9.823	4.443
r_E	µgCµg^{-1}Cd^{-1}	0.204	0.525	0.832	0.563
K_{dorm}	µgC g^{-1}	948	5734	10265	671
p_{BD*}	µgC µg^{-1}C	0.066	0.691	1.293	1.757
p_{BH*}	µgC µg^{-1}C	6.709	8.653	9.782	0.229
p_{BI1*}	µgC µg^{-1}C	0.236	3.253	9.337	0.235
p_{BI2*}	µgC µg^{-1}C	0.350	3.074	6.678	5.474
γ	-	0.07	0.49	1.83	0.27
τ	-	0.45	0.76	0.98	0.98
pE_D	-	0.131	0.439	0.874	0.045
pE_H	-	0.005	0.038	0.078	0.030
$p_{I2,en}$	-	0.069	0.782	1.746	0.477
r_0	-	fixed	fixed	fixed	0.9
β	-	fixed	fixed	fixed	0.01
$S_{I2,ex}$	µgC g^{-1}	fixed	fixed	fixed	1800

* The parameter depends on other parameters in a Dirichlet distribution.

3.2.4 Simulating effect of only dissolvable, hot water extractable or insoluble carbon applications

Following model calibration and validation, we run three simulations to explore the hypothetical impacts of applying pure D, H and I substances to the soil. We simulated the application of 150 mg (3 mg g^{-1} soil) for each fraction to investigate their individual contributions to changes in carbon pools and fractions, microbial biomass changes and priming effects. This provides insight into the control that the model attributes to these components in driving soil carbon dynamics.

3.2.5 Fourier Amplitude Sensitivity Testing

We performed a global sensitivity analysis via Fourier Amplitude Sensitivity Testing (FAST). FAST is a variance-based method that efficiently explores the impact that parameter variations have on the performance of nonlinear mathematical models (Henkel, Wilson, and Krug 2012; Reusser, Buytaert, and Zehe 2011). This sensitivity test allowed further insight into the model behaviour and the relative importance of different parameters in determining model predictions. This information was used to identify which of the mechanisms included in the MiPrime conceptual framework are the most important drivers of soil carbon dynamics.

Reliable parameter sensitivity information with FAST requires a sufficient number of FAST iterations. To determine the number of iterations required, we applied the following equation (3.33; Henkel et al. 2012):

$$N = \left(1 + 4M^2(1 + (k-2)d)\right)k \qquad (3.33$$

Where N is the minimum number of parameter iterations; M is the inference factor (default $M = 4$); d is the frequency step (default $d = 2$) and k is the number of model parameters (Houska 2015). With $k = 28$ for the 28 free parameters described in Table 3.4, we calculated that we needed $N = 95{,}004$ iterations for reliable results with FAST.

3.3 RESULTS

3.3.1 Model performance on data used to calibrate the model

Model predictions for data used in model calibration (i.e. data from grasses, fermented grasses and composted grass treatments**)** demonstrate a generally close fit with the observed total, mineralized, microbial biomass and primed carbon concentrations (Figure 3.3.1 and Figure 3.3.2) and the Dissolvable (D), Hot water extractable (H) and Insoluble (I) carbon concentrations (Figure 3.4.1 and Figure 3.4.2).

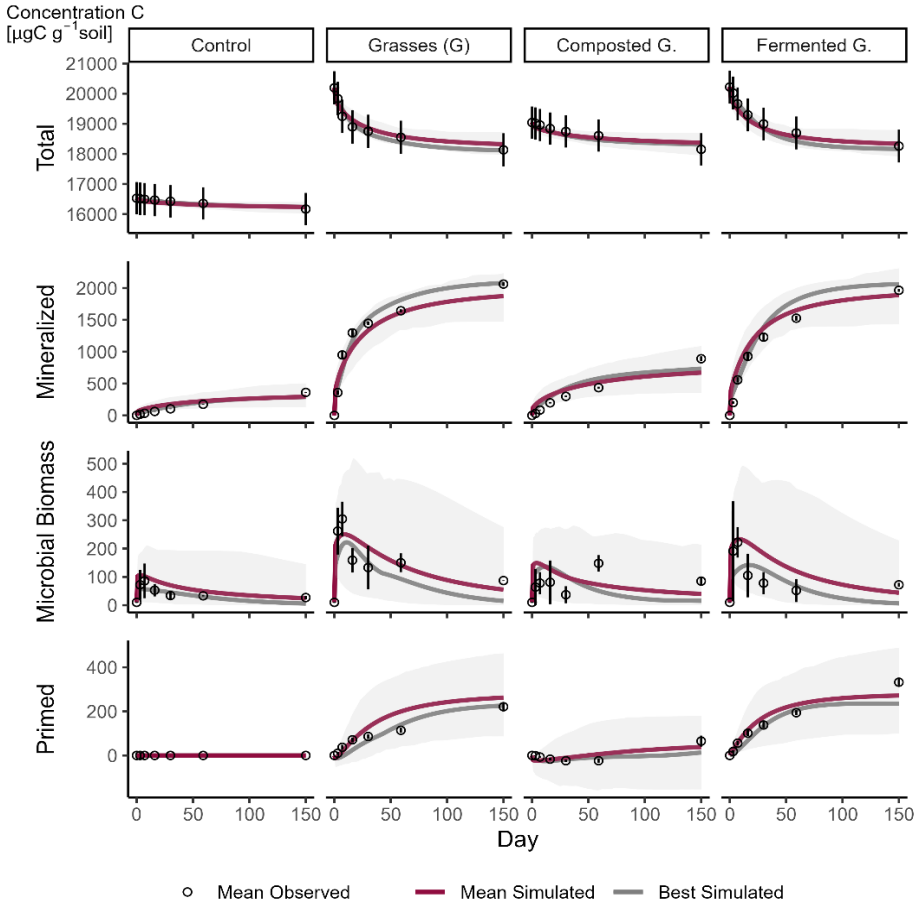

Figure 3.3.1 Model simulation and observed data for total, mineralized, microbial biomass and cumulative primed carbon concentrations (per gram soil) over time after amending a podzol with grasses, composted grasses, fermented grasses and no organic amendment (control). These concentrations do not distinguish between contributions from EX and EN pools, but rather represent their combined contribution. Supplementary figures N1 and N3 show the EX and EN contributions, respectively. The shaded area denotes the 5% and 95% certainty quantiles.

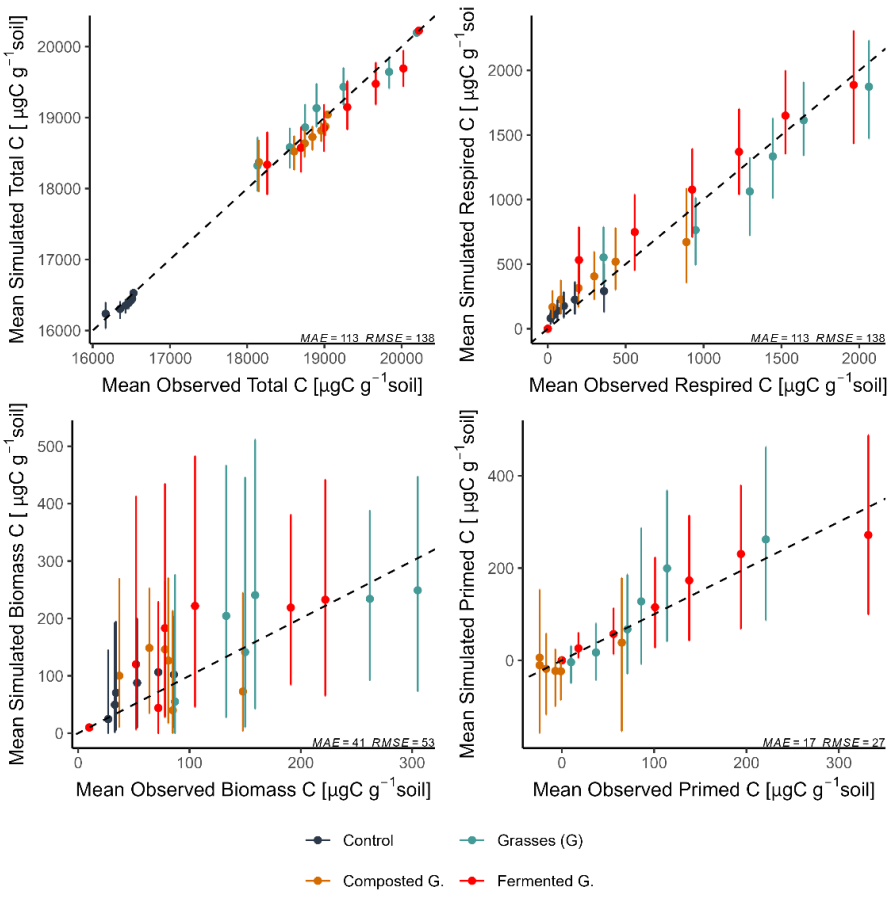

Figure 3.3.2 Model simulation and observed data for total, mineralized, microbial biomass and cumulative primed carbon concentrations (per gram soil) over time after amending a podzol with grasses, composted grasses, fermented grasses and no organic amendment (control). These concentrations do not distinguish between contributions from EX and EN pools, but rather represent their combined contribution. Supplementary figures N1 and N3 show the EX and EN contributions, respectively. The dashed line in observed vs. simulated plots is the line of perfect fit (1:1 match of observed to simulated data).

The reverse Michaelis-Menten functions can reproduce the observed trends for total carbon accurately, but the simulation of respired and primed carbon appears to lose accuracy at later time steps. Model simulations of microbial biomass are relatively accurate for the simpler trends observed for the control and fermented grasses treatments, which display an initial sharp increase followed by a decline, but the model has more difficulty capturing the more complex behaviour observed for biomass growth in grasses and composted grasses

treatments, which additionally exhibit a second phase of microbial biomass growth around day 60 (Figure 3.3).

The model is well able to simulate changes in individual D, H and I carbon concentrations, matching with differing accuracies the experimental data (Figure 3.4.1 and Figure 3.4.2). Model performance is suboptimal in simulating H fractions compared to other fractions, and especially at later time steps, model predictions increasingly overestimate H concentrations remaining in the soil.

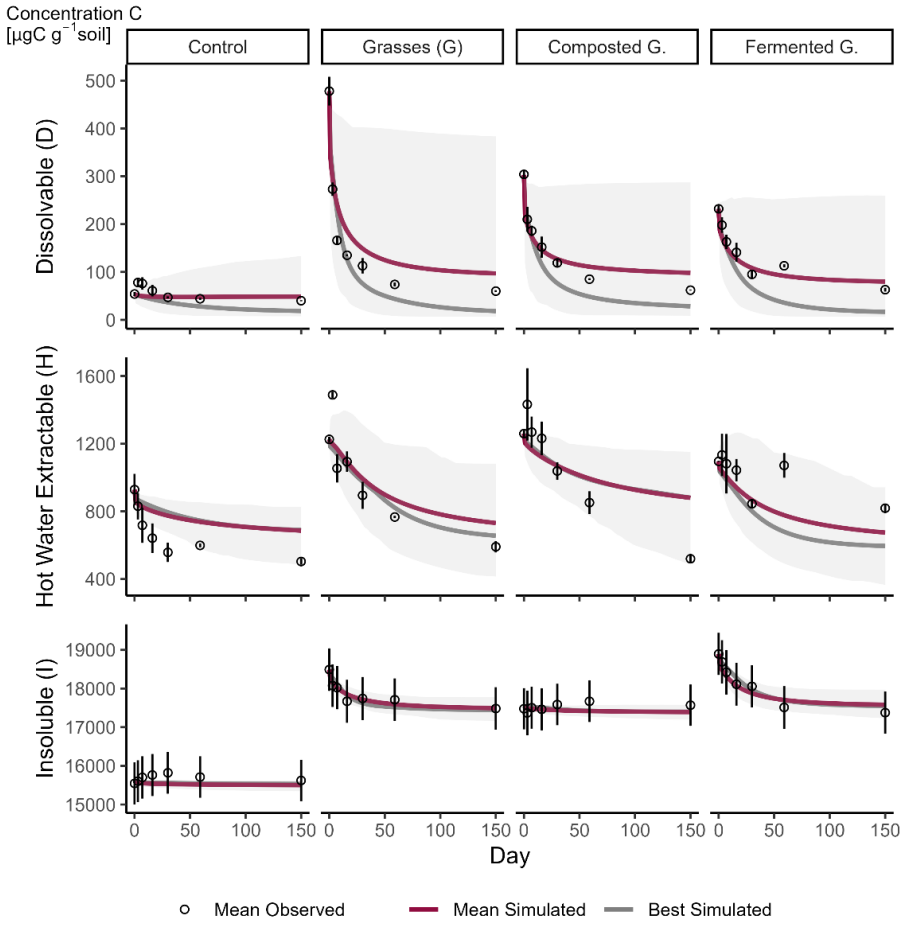

Figure 3.4.1 Model simulation and observed data for Dissolvable (D), Hot water extractable (H) and Insoluble (I) carbon concentrations (per gram soil) over time after amending a podzol with grasses, composted grasses, fermented grasses and no organic amendment (control). These concentrations do not distinguish between contributions from EX and EN pools, but rather represent their combined contribution. Supplementary figures N2 and N4 show the EX and EN contributions, respectively. The shaded area denotes the 5% and 95% certainty quantiles.

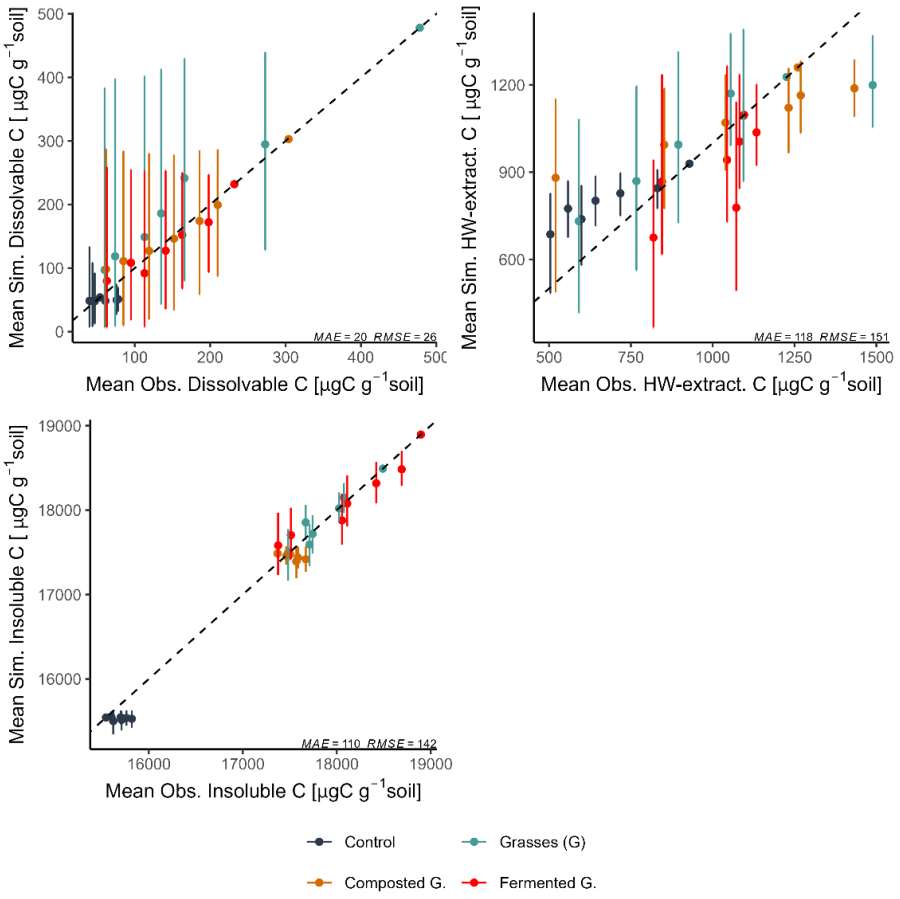

Figure 3.4.2 Model simulation and observed data for Dissolvable (D), Hot water extractable (H) and Insoluble (I) carbon concentrations (per gram soil) over time after amending a podzol with grasses, composted grasses, fermented grasses and no organic amendment (control). These concentrations do not distinguish between contributions from EX and EN pools, but rather represent their combined contribution. Supplementary figures N2 and N4 show the EX and EN contributions, respectively. The dashed line in observed vs. simulated plots is the line of perfect fit (1:1 match of observed to simulated data).

Simulation of the calibration data shows that the model is able to better simulate changes in exogenous carbon concentrations than endogenous carbon concentrations (Supplementary Figures N1-N4). For the endogenous pool, especially changes in total and respired carbon concentrations appear significantly more linear over time than the model is able to predict with its Michaelis-Menten-type functions (Figure S4).

3.3.2 Model performance on data not used for model calibration

Validation of model performance by comparing model predictions to a testing dataset not used for model calibration (i.e. data from woodchips and waterway residues treatments) show that the model is able to predict changes in total, mineralized, microbial biomass and primed carbon concentrations generally well, though overestimating the microbial biomass growth and respiration rates for wood chips application (Figure 3.5). While, for the wood chips treatment, the model struggles to predict the linear response of the microbial respiration over time, predicted changes in total carbon concentrations are generally accurate for waterway residues (RMSE=282 μgC g^{-1} soil; Figure 3.5).

As observed for the calibration data, the model is able to predict changes in D, H and I fractions over time with reasonable accuracy (Figure 3.6). Yet, here too, the model shows difficulty in predicting changes in the H fraction. The I fraction shows increasing deviation of modelled versus observed concentrations for longer-term changes (t>50 days). Changes in the D fraction appear more predictable, given their consistent, rapid decline across all organic amendment treatments. The decomposition of carbon fractions in exogenous and endogenous carbon pools are predicted to be generally similar for both wood chips and waterway residues (Supplementary Figures N5-N8).

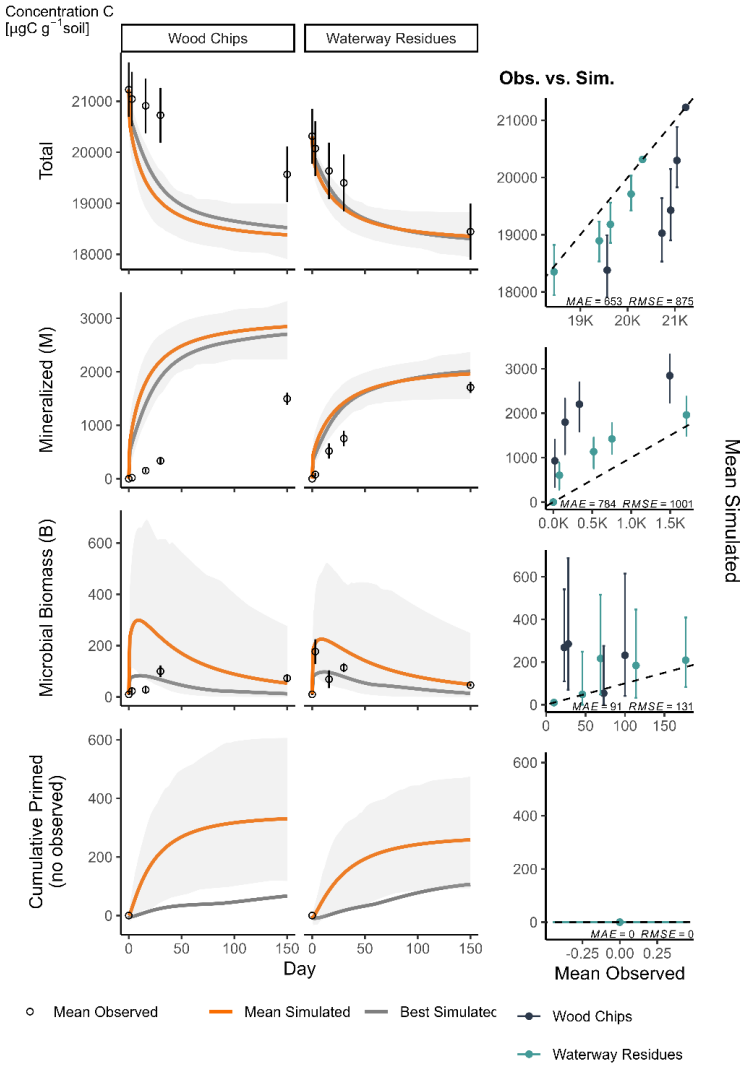

Figure 3.5 Model predictions and observed data for total, mineralized, microbial biomass and primed carbon concentrations (per gram soil) over time after amending a podzol with wood chips and waterway residues. These concentrations do not distinguish between contributions from EX and EN pools, but rather represent their combined contribution. Supplementary figures N5 and N7 show the EX and EN contributions, respectively. The shaded area denotes the 5% and 95% certainty quantiles. The dashed line in observed vs. simulated plots is the line of perfect fit (1:1 match of observed to simulated data). There is no observed data for the cumulative primed carbon.

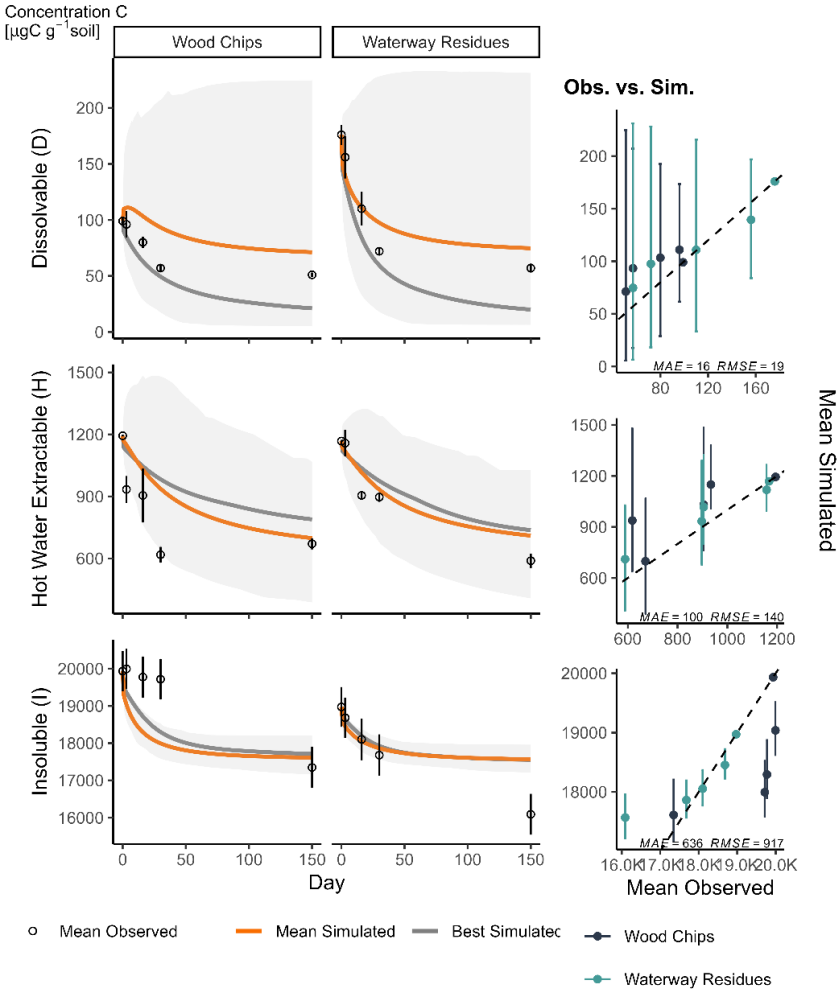

Figure 3.6. Model predictions and observed data for total Dissolvable (D), Hot water extractable (H) and Insoluble (I) carbon concentrations (per gram soil) over time after amending a podzol with wood chips and waterway residues. These concentrations do not distinguish between contributions from EX and EN sources, but rather represent their combined contribution. Supplementary figures N6 and N8 show the EX and EN contributions, respectively.

3.3.3 Effect of hypothetical, pure D, H and I amendments

Simulation of applying pure D, H and I substances reveal differences in the model-predicted impacts on carbon pools and fractions, microbial biomass and primed carbon (Figure 3.7). Notable differences are that the application of the D-substance resulted in slightly higher biomass growth and greater priming effects, whereas the H-substance was the only substance to induce a strong negative priming effect.

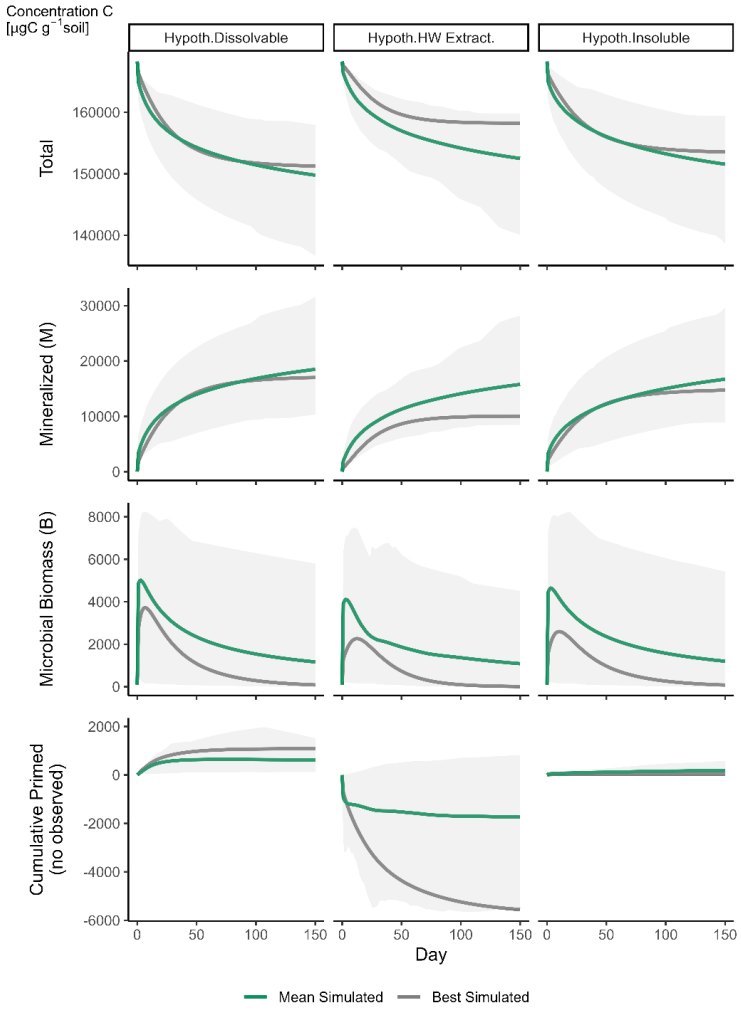

Figure 3.7 Model predictions for total, mineralized, microbial biomass and primed carbon concentrations (per gram soil) over time after hypothetical application of pure D_{ex}, H_{ex} and I_{ex} substances to the podzol. The shaded area denotes the 5% and 95% certainty quantiles. Supplementary figures N9 and N11 show the EX and EN contributions, respectively.

3.3.4 Sensitivity Analysis

FAST shows strong variations in the influence of different parameters on model predictions but highlights that model results are particularly sensitive to the parameters related to the insoluble (I) carbon pool, such as the maximum decomposition rates of I_1 and I_2 ($Q_{I1,}$ Q_{I2}), the Michaelis-Menten constant for I_2 (K_{I2}), and the initial size of the I_2 fraction in amendments ($S_{Iex,2}$; Figure 3.8). Also, the relative loss rate of extracellular products such as enzymes (r_E) has a relatively stronger influence on model predictions. Notable is also the model's relative insensitivity to variations in the parameters related to the dissolvable (D) fraction.

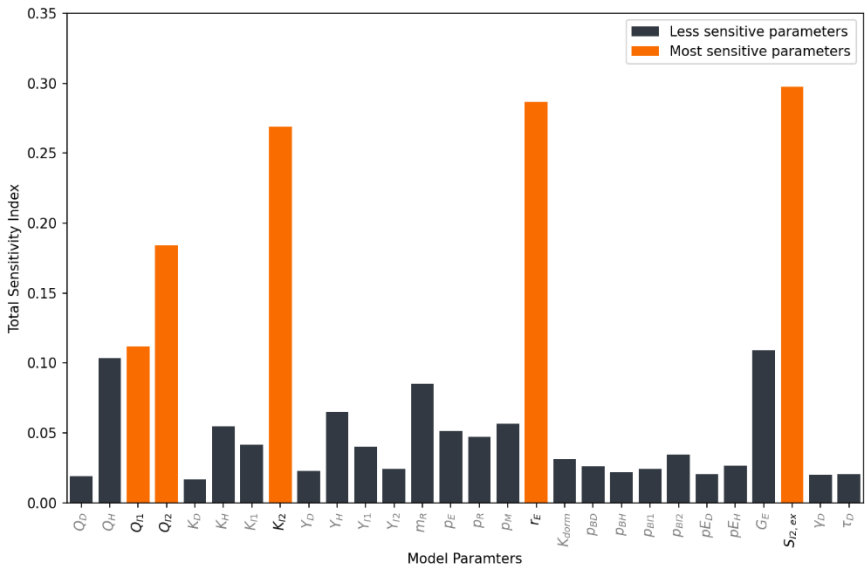

Figure 3.8. Fourier Amplitude Sensitivity Test (FAST) with the top five most influential parameters highlighted in orange. Values show the contribution of each parameter to the overall variation in the model output and thus provide an indication of the importance of each parameter to model performance.

3.4 DISCUSSION

The calibration and validation of MiPrime, based on the application of five compositionally distinct organic amendments, demonstrates that the model is able to describe soil carbon dynamics in terms of changes over time in (i) total, mineralized, microbial biomass and primed carbon and (ii) dissolvable (D), Hot water extractable (H) and Insoluble (I) carbon fractions, with good accuracy for a diversity of organic amendments (Figure 3.3, Figure 3.4, Figure 3.5, Figure 3.6). These results suggest that the MiPrime model can be a good alternative to many existing carbon models by allowing for an assessment of short-term organic amendment impacts on multiple, measurable carbon fractions through mechanistic processes. Yet, the model also exhibits weaknesses that lie especially in predicting changes in carbon mineralization rates and changes in endogenous carbon fractions. The experimental data demonstrate that changes in these components have, in contrast to other pools and fractions and at least in the short term, a more linear response than the Michaelis-Menten-type response imposed in MiPrime. These shortcomings, as well as model successes, however, provide several interesting insights into key soil processes related to soil carbon dynamics that are further discussed below.

3.4.1 Use of measurable organic carbon fractions

The MiPrime model distinguishes differences and changes in organic matter based on differences in the decomposability of measurable dissolvable (D), hot water extractable (H) and insoluble (I) carbon fractions. The choice for these fractions was inspired by the forest litter decomposition model YASSO, wherein different carbon fractions are discerned, aimed at isolating different biogeochemical components of forest litter (Liski et al., 2005). However, experimental studies have shown that wet chemical extractions designed to isolate specific organic components often include a wide range of other substances as well, depending on the fraction and the organic amendment type (McKee et al. 2016; Preston et al. 1997; Preston and Trofymow 2015). For example, lignin extractions, based on the same wet-chemical extraction principles applied here, evidentially include other types of compounds such as tannins, cutin or suberin (Preston and Trofymow 2015). Results from the MiPrime model could similarly be interpreted to indicate a chemical heterogeneity of D, H and I fractions. Noticeable points of inflection for some of the curves, especially for the D and I fractions, could indicate that these fractions might contain components that decompose much more rapidly and components that barely decompose at all (Figure 3.4). For the I fraction, the slower parts were separated by the model from the fast-decomposing parts through the $S_{I2,ex}$ and $p_{I2,en}$ parameters, allowing the model to function quite well. Validation with wood chips and waterway residues (Figure 3.6) shows that the size of the non-decomposing part of the I fraction is, as expected, not constant for all organic

amendments and is likely much smaller for these non-grass derived organic amendments. These findings suggest that further dissection of the I fraction is necessary to avoid the need for these artificial parameters.

The D pool similarly displays behaviour suggestive of chemical heterogeneity. In the endogenous pool, for instance, the D fraction exhibits a phase of rapid increase for the duration that the decomposition in the exogenous pool is greatest (Figure N4). This contrasts observations for the D fraction in the exogenous pool where the D fraction is rapidly decomposed (Figure N2). The increase in D in the endogenous pool hints at a rapid release of enzymes from the soil pool aimed at degrading the freshly introduced organic amendments. The rapid decrease of endogenous I, in all except for control soils, suggests that the increase in D is derived from a transformation of I, which contradicts the notion that the entirety of soil I present at the start of the experiment is relatively inaccessible or difficult to decompose.

The inability of MiPrime to accurately capture these dynamics suggests that the representation of D, H and I pools is likely too simplistic still and that other or additional pools are required for a yet more accurate simulation of changes in all soil carbon fractions. Nevertheless, the current modelling exercise demonstrates that, even though the different solubility fractions may capture more compounds than originally intended, these fractions still provide a good characterization of organic matter for the adequate prediction of general SOM degradation kinetics.

3.4.2 Labile versus recalcitrant

Studies have generally emphasized the importance of what is traditionally referred to as labile carbon fractions (i.e. D and H) in driving decomposition trends (Bradford, Fierer, and Reynolds 2008; De Graaff et al. 2010). Fourier Amplitude Sensitivity Testing of our model shows, however, that model results are especially sensitive to variations in parameters related to the I fraction (Q_{I1}, Q_{I2}, K_{I2}, $S_{Iex,2}$). This sensitivity likely derives partly from the relative size of the I fraction, as this is on the order of 10-15 times greater than combined D and H fractions. Nevertheless, the high sensitivity of model performance to variations in parameters related to the I fraction suggests that potentially more attention is warranted for microbial interactions with resistant carbon fractions than is done so far.

3.4.3 Priming effects

Priming effects could not be assessed for the organic amendments of natural isotopic abundance. Nevertheless, the calibration results show that MiPrime was able to capture differences in the direction of priming effects for the various organic amendments, simulating positive priming effects for grasses and Bokashi and negative priming effects for

compost. Defining the microbial preferentiality for carbon within either the exogenous or endogenous pool based on the difference in the hot-water carbon concentrations between each pool (Kok et al., 2022) was thus sufficient to determine the direction of the priming effect. This is confirmed in the simulation of hypothetical pure applications of D, H and I substances, where negative priming effects were observed for H substances, and minor positive priming effects for D and I substances. For pure D substances (e.g. sugar), both negative priming effects (Kuzyakov and Bol 2006) and positive priming effects have been observed in other studies (Nottingham et al. 2009). The amount of amendment applied (Zhu et al. 2022) and soil properties (Liu et al. 2020; Yan et al. 2023) may explain this variation, as the amount applied, the concentration of soil carbon fractions and the presence or absence of other fractions in the amendments (thereby reducing or increasing the H concentration) also influence the direction and magnitude of the priming effect.

While general priming trends are well captured, the model also has some inaccuracies in its priming predictions. For instance, both positive priming effects for grasses and Bokashi are predicted to be of very similar magnitude, while the experimental data demonstrates that, especially at later time steps, the priming effect for Bokashi becomes greater than that of grasses (Figure 3.3). The priming effects for wood chips and waterway residues similarly show only minor differences in magnitude, despite their distinctly different chemical compositions. As MiPrime does not account for nitrogen, we may expect it to underestimate biomass growth and overestimate carbon mineralization for woodchips, as microorganisms are not constrained by the usual lack of nitrogen due to the high C:N ratio of wood. Finally, because the model has a bias towards better predicting changes shortly after organic amendment application (due to the higher sampling density in the early phases of the experiment), MiPrime largely underestimates the magnitude of late-stage priming effects (i.e. $t>50$ days).

Priming is complex, and even models based on operationally defined pools (e.g. PRIM) are "not able to fully catch the observed variability of priming" (Guenet et al. 2016). ORCHIMIC performs better in estimating the priming effect, though this has been tested only against the addition of pure cellulose (Huang et al. 2018). ORCHIMIC's validation data demonstrates a brief negative priming effect ($t<25$ days) for cellulose before becoming positive for the remainder of the experiment (Blagodatskaya et al. 2014). This is similar to our observations for compost, though we observed our compost's negative priming phase to last longer, until approximately $t=60$ days. While ORCHIMIC captures this trend, it largely underestimates the magnitude of the negative phase of cellulose's priming effect. For a similar time period as ORCHIMIC, MiPrime was able to capture the direction and magnitude of the priming effect for three compositionally diverse organic amendments using 31 parameters (as opposed to ORCHIMIC's 61 parameters - though including temperature effects, among other).

3.4.4 Static linearity

Decomposition in MiPrime is described through a reverse Michaelis-Menten function (Buchkowski et al. 2017). However, changes in endogenous carbon fractions and late-stage carbon respiration rates (and thus also priming rates), in several cases, appear insensitive to changes in microbial biomass and enzyme concentrations, demonstrating linear rather than asymptotic trends over time (Figure 3.5 and Figures N3 and N4). The model is unable to rationalize how respiration rates are not near exponential when the decomposition rates and changes in biomass are. There are several mechanisms that might explain this disconnect, such as i) the establishment of two or more separate microbial communities that have limited interaction with each other, or ii) the growth of different, specialized microbial populations within the larger community.

By the first mechanism, the colonization of the organic amendment might result in the establishment of a new, organic amendment-constrained microcolony that has very little interaction with the old soil community. This can be rationalized considering the spatial scales at which microorganisms operate, and given that microorganisms are strongly influenced only by the physical and chemical environment directly adjacent to them (Parkin 1993). These interactions likely take place in the order of micrometres (~10 μm) to nanometres, and thus, a community rapidly colonizing organic amendment particles may become spatially isolated from the old soil community. Only for those microorganisms operating at the interface between both pools, or when soil moisture diffuses this interface and forces an exchange of microorganisms and nutrients between both pools, there is some interaction of the organic amendment with the old community resulting in priming effects. Implementing such a mechanism in MiPrime would imply that at least two biomass and enzyme pools would need to be introduced to represent a separate microbial community for the endogenous and exogenous pools, respectively.

By the second mechanism, an exchange of nutrients might take place between pools, and the community may operate as a single entity, but differences in community composition may arise due to the growth of microbial populations with physiological features that are functionally distinct from the original microbial population. In this situation, the community existing prior to organic amendment application, consisting mostly of specialized microorganisms able to survive under the possibly limited nutrient conditions, will mostly ignore the organic amendments introduced, as they cannot compete with the growth of opportunist microorganisms that rapidly feed off the newly available substrate. These fast growers, in turn, likely ignore the potentially limited or difficult-to-access original nutrients still in the soil. These mechanisms are well explored conceptually (Fierer, Bradford, and Jackson 2007; Ho, Di Lonardo, and Bodelier 2017; Roller and Schmidt 2015), yet are limitedly applied in models given their added complexity. In MiPrime, for instance, distinguishing between different microbial populations and their unique

behaviours in response to the various soil carbon fractions would imply adding at least a second pool of biomass, one for each physiologically distinct subpopulation, as well as the definition of a second set of Q_F, $K_{F,}$ $\eta_{F,}$ η_E parameters and all others characterizing the behaviour of each. Though coming at a trade-off in compounding the number of model parameters, including some dimension of microbial diversity, at either a biomass level (Blagodatsky and Richter 1998), an enzymatic level (Allison 2012), or otherwise, undeniably results in models that better reflect the realistic complexity of decomposer communities.

3.4.5 Relationships with the POM-MAOM conceptualization of soil organic matter

Recent years have seen the popular adoption of SOM separation into particulate (POM) and mineral-associated (MAOM) fractions (Cotrufo et al. 2019). Here, POM is generally defined as consisting of organic fragments that are relatively undecomposed, while MAOM consists of predominantly mineral-associated derivative products created through the chemical transformation of POM by soil microorganisms (Lavallee, Soong, and Cotrufo 2020). POM-MAOM separation is generally achieved by separating SOM into physical size fractions rather than chemically, as is done for MiPrime. Though MiPrime employs a different conceptual framework, it shares many similar processes defined in the POM-MAOM framework. MAOM, for instance, is created through one of two pathways. Firstly, the "ex vivo modification pathway", where MAOM forms as plant litter leachate or depolymerized exoenzymes directly associated with the mineral phase (Liang, Schimel, and Jastrow 2017). This pathway partially coincides with MiPrime's 'enzyme loss flux' from the enzyme pool to the soil pool in the MiPrime schematic, where a portion of exo-enzymes is lost each day and subsequently integrated into the D and H fractions of the soil pool (Figure 3.1). MAOM also forms through "in vivo microbial turnover pathways", such as through necromass accumulation (Liang et al. 2017). This coincides with MiPrime's microbial mortality flux from the biomass pool to the soil pool (Figure 3.1). Importantly, however, MiPrime does not stabilize these compounds through mineral associations and is in that way different from MAOM. Mineral association can saturate, and MiPrime does not allow for a saturation of the soil pool. Rather, MiPrime stabilizes transformed compounds through the Michaelis-Menten function where, essentially, if the concentration in enzymes is too low due to a lack of readily available substrates, then decomposition becomes strongly inhibited and organic matter is 'stabilized'. MiPrime pool definitions similarly do not contradict the POM-MAOM framework either. The MiPrime amendment pool largely consists of POM that can be preserved for decades due to the chemical resistance of the I_2 fraction of organic amendments. In this regard, MiPrime reflects the understanding of the POM-MAOM framework in that it allows for carbon stabilization through ex vivo modification and in vivo turnover pathways, as well as the selective preservation of POM.

To conclude, because POM-MAOM are often applauded as the best way forward to understand and predict broad-scale SOM dynamics (Lavallee et al. 2020), it would be interesting for future investigations to explore how MiPrime's fractions relate to POM-MAOM fractions, and/or to include well established POM-MAOM mechanisms (e.g. mineral associations and their saturation) in the MiPrime framework.

3.4.6 Further development

MiPrime offers an initial step towards the mechanistic modelling of changes in measurable soil carbon fractions and associated priming effects, but it can be further improved in numerous respects. The field application of this model would benefit from the inclusion of, for instance, i) a nitrogen component, as decomposition is influenced by the stoichiometric balance between the nutrients and microorganisms (Goll et al. 2017; Manzoni and Porporato 2009; Mooshammer, Wanek, Zechmeister-Boltenstern, et al. 2014; Sinsabaugh and Follstad Shah 2012); ii) an expression of microbial diversity, given that different microorganisms exhibit different life strategies that can contrastingly affect decomposition (Allison et al. 2013; Bending et al. 2002; Condron et al. 2010; Creamer et al. 2015); iii) the inclusion of soil physical protection mechanisms and mineral associations (e.g. MAOM), as also the physical accessibility of microorganism to carbon will influence the rate of decomposition (Cotrufo et al. 2013; Lehmann and Kleber 2015; Luo, Baldock, and Wang 2017; von Lützow et al. 2008; Wang et al. 2022); iv) further dissection of the I pool to remove the need for artificial parameters separating I_1 and I_2; and finally, iv) the inclusion of environmental parameters, defined by properties such as soil type, soil moisture and temperature, which can also affect microbial activity. The consideration of including such components, however, will warrant a careful weighing of trade-offs between increasing model parameters and complexity versus gains in model performance. The complexity of the soil system is, after all, difficult enough to incorporate into a single conceptual model, let alone into a tractable yet accurate numerical model (Schmidt et al. 2011).

3.5 CONCLUSION

MiPrime introduces a mechanistic approach to modelling microbially mediated soil carbon dynamics, including priming effects, based on empirical pools that are quantifiable through parsimonious soil extraction methods. The model was able to simulate changes in carbon fractions in both exogenous (i.e. organic amendment-derived) and endogenous (i.e. soil-derived) pools with reasonable accuracy for five compositionally diverse organic amendments, including three types of roadside grasses, wood chips and water weeds and reeds. For the isotopically labelled organic amendments, the model performed well in capturing variations in the magnitude and direction of short-term priming effects. MiPrime

thus contributes to the development of models predicting carbon dynamics in response to the addition of a variety of complex organic amendments based on largely measurable carbon fractions. MiPrime offers a step towards bridging the divide between models developed to understand the mechanisms governing soil carbon dynamics and models designed to address practical questions regarding the design of effective land management strategies.